

Nanoscale

Accepted Manuscript



This is an *Accepted Manuscript*, which has been through the Royal Society of Chemistry peer review process and has been accepted for publication.

Accepted Manuscripts are published online shortly after acceptance, before technical editing, formatting and proof reading. Using this free service, authors can make their results available to the community, in citable form, before we publish the edited article. We will replace this *Accepted Manuscript* with the edited and formatted *Advance Article* as soon as it is available.

You can find more information about *Accepted Manuscripts* in the [Information for Authors](#).

Please note that technical editing may introduce minor changes to the text and/or graphics, which may alter content. The journal's standard [Terms & Conditions](#) and the [Ethical guidelines](#) still apply. In no event shall the Royal Society of Chemistry be held responsible for any errors or omissions in this *Accepted Manuscript* or any consequences arising from the use of any information it contains.

Giant Tunnel Magneto-Resistance in Graphene Based Molecular Tunneling Junction

Bin Wang,^a Jianwei Li,^a Yunjin Yu,^a Yadong Wei,^{*a} Jian Wang,^{*b} and Hong Guo^c

We propose and theoretically investigate a class of stable zigzag graphene nanoribbon (ZGNR) based molecular magnetic tunneling junctions (MTJs). For those junctions having pentagon-connecting formation, huge tunnel magneto-resistance (TMR) is found. Different from most of the other proposed molecular junctions, the huge TMR in our structures is generic, which is not significantly affected by external parameters such as bias voltage, gate voltage, length of the molecule and width of ZGNRs. The double pentagon-connecting formation between the molecule and ZGNRs is critical for the remarkable TMR ratio, which is as large as $\sim 2 \times 10^5$. These molecular MTJs behave as almost perfect spin filters and spin valve devices. Other connecting formation of the ZGNR based MTJs leads to much smaller TMR. By first principles analysis, we reveal the microscopic physics responsible for this phenomenon.

1 Introduction

Tunnel magneto-resistance (TMR) is an important phenomenon which has become a device principle for many electronic applications such as magnetic sensors and magnetic random access memory^{1,2}. In a magnetic tunneling junction (MTJ) made of two ferromagnetic metals sandwiching a thin insulator, TMR describes the resistance variation when magnetic moments of the two metals change from parallel configuration (PC) to anti-parallel configuration (APC). One of the principle aspects of MTJ research is to obtain large TMR because it can provide higher sensitivity for practical applications. In traditional MTJ, the magnetic metals are usually Fe, Co, Ni and their alloys, and the insulators are typically Al_2O_3 and MgO. TMR value $\sim 12\%$ was firstly detected in $\text{CoFe}/\text{Al}_2\text{O}_3/\text{Co}$ ³ MTJ and $\sim 18\%$ in $\text{Fe}/\text{Al}_2\text{O}_3/\text{Fe}$ ⁴ MTJ at room temperature. The value was further enhanced to $\sim 30\%$ in the MTJ composed by $\text{Fe}/\text{Co}/\text{Ni}$ alloys with Al_2O_3 barrier.⁵ TMR value up to 220% were observed in single crystal Fe-MgO-Fe MTJ at room temperature^{6,7} and is proved can be further enhanced by strain of the device.⁸ Recently, TMR as large as 1100% at low temperature and 600% at room temperature has been experimentally reported in $\text{CoFeB}/\text{MgO}/\text{CoFeB}$ MTJs,⁹ although this value is still much smaller than that predicated by first principles calculation.^{10,11}

More recently, TMR in *molecular* MTJs has received much attention since quantum transport properties can be chemically exploited for better and novel functionality.¹²⁻¹⁴ Mahato R.N. *et.al* reported an exceptionally large ($> 2000\%$) TMR value in one-dimensional systems formed by molecu-

lar wires embedded in a zeolite host crystal experimentally.¹² They emphasize that the ultrahigh TMR value is attributed to spin blockade in one-dimensional electron transport. Theoretically, several groups predicted very large TMR values in different *molecular* MTJ.¹⁵⁻¹⁹ Rocha *et al.* calculated TMR in Ni-tricene-dithiolate-Ni molecular structure and predicted a significant TMR value, $\sim 600\%$.¹⁵ Zu *et al.* investigated spin-polarized transport of magnetic-Fe4 molecules in contact with two gold electrodes.¹⁶ Even though gold electrodes are not magnetic, due to the magnetic property of Fe4, a large TMR value $\sim 1800\%$ was predicted. Ni *et al.*¹⁷ investigated perylene tetracarboxylic diimide molecules sandwiched between two graphene nanoribbons and theoretically predicted a huge TMR $\sim 10^4\%$. Cao *et al.*¹⁸ studied Fe-terminated zigzag graphene nanoribbon (ZGNR) junction using first-principles method and found TMR ratio can reach more than $\sim 10^5\%$.

In these works¹⁵⁻¹⁷, the large TMR was due to very sharp transmission resonances, in other words, the alignment or miss-alignment of a resonance to the Fermi level causes a large change in tunneling. We note that the phenomenon of resonance mediated large TMR is inevitably sensitive to device details. Namely a small variation in the contact structure during device fabrication is enough to shift the narrow energy bands near the Fermi level which destroys the desired TMR. While one may carefully control such contact details in a research laboratory, it would be extremely hard - if not outright impossible, to reach such a high degree of control in large scale practical fabrication.

Therefore, a very important next step is to understand device contacts thereby finding favorable structures for realizing the large TMR in molecular MTJ in a robust way. To this end, one notes that graphene possesses outstanding properties including high carrier mobility and long spin relaxation length.²⁰⁻²² ZGNR can be processed to have a large spin polarization on account of quantum confinement and edge effect.²³ Due to chemical similarity, it is natural that graphene

^a College of Physics Science and Technology, Shenzhen University, Shenzhen, 518060, China. E-mail: ywei@szu.edu.cn; Fax: +8675526538735; Tel: +8675526535355

^b Department of Physics, the University of Hong Kong, Hong Kong, China; The University of Hong Kong Shenzhen Institute of Research and Innovation, Shenzhen, China. E-mail: jianwang@hku.hk.

^c Department of Physics, McGill University, Montreal, Canada.

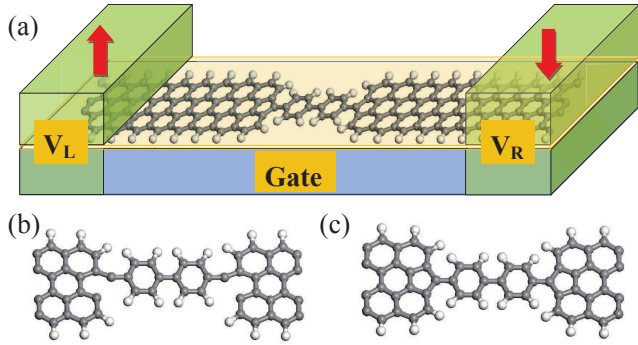


Fig. 1 (Color online) (a) Schematic structures of the ZGNR based MTJ, where a biphenyl molecule ($M=2$) is connected by two semi-infinite ZGNRs with width $N=4$. The carbon atoms at both edges of ZGNRs are mono-saturated by hydrogen atoms. Green bulks indicate the lead regions where bias voltage V_L and V_R are applied. Blue bulk represents the voltage gate in the scattering region. Red arrows describe the orientation of external magnetic fields in leads. Two different connecting configurations between biphenyl molecule and ZGNRs are given in (b) and (c). The former is named as double dangling-connecting formation and the latter is named as double pentagon-connecting formation. Six ZGNR unit cells in each lead are used as buffer layers in the scattering region.

can easily form chemical bonds to organic molecules. Therefore, ZGNR based molecular MTJ¹⁷ is very interesting and important, and spin polarized transports in such MTJs have also received tremendous attention^{18,24,25}.

In this work, we theoretically investigate and search for proper ZGNR/molecule contacts that lead to giant TMR values not relying on quantum resonance. We found a class of stable ZGNR bridging polyphenyl molecules and, for those junctions having pentagon-connecting formation, giant TMR is found. Importantly, the giant TMR is generic and not significantly affected by external parameters such as bias voltage, gate voltage, length of the molecule and width of ZGNRs. The double pentagon-connecting formation between the molecule and ZGNRs is critical for the remarkable TMR ratio - as large as 2×10^5 ($\sim 2 \times 10^7\%$). These molecular MTJs behave as almost perfect spin filters and spin valve devices. Other connection formation, however, leads to much smaller TMR. By first principles analysis, we reveal the microscopic physics responsible for this phenomenon.

2 Computational details

Fig.1(a) is the schematic structure of ZGNR based MTJ where a biphenyl molecule is sandwiched between two mono-hydrogenated semi-infinite ZGNRs. Two different connecting formations between biphenyl molecule and ZGNRs were investigated. In the first formation as shown in Fig.1(b), the

phenyl group connects to both ZGNR leads by sp hybrid orbitals which is hereafter referred to dangling structure. In the second formation as shown in Fig.1(c), the phenyl group connects to each ZGNR lead by sp^2 hybridization which is named as pentagon structure. Both structures are relaxed by VASP²⁶ and numerical results indicate that pentagon structure is more stable than dangling structure.²⁷ Previous investigation indicated that ZGNR has spontaneous magnetic moments with spin orientations on both edges parallel or anti-parallel.^{28,29} The total magnetic moment is zero in spin anti-parallel configuration and non-zero in spin parallel configuration. In this paper, only the parallel configuration of ZGNR is considered because magnetic field is applied on each lead in order to investigate TMR behaviors. We note that all the ingredients of the device are carbon atoms and the ZGNR structure has been fabricated experimentally with width as narrow as 2 nm^{30,31} making the proposed device easier for experimental realization.

Quantum transport properties of molecular devices were performed by first principles package NanoDCal^{32,33} which is based on the standard NEGF-DFT method^{34,35}. Double- ζ basis^{36,37} set was used to expand the wave functions and the exchange-correlation potential was treated at LSDA level³⁸⁻⁴⁰. The mesh cut-off energy was 200 Rydberg and energy tolerance for self-consistency was restricted to 10^{-4} eV.

The spin resolved transmission coefficient is calculated by

$$T_{\sigma}(E) = \text{Tr}[\Gamma_L(E)G^r(E)\Gamma_R(E)G^a(E)]_{\sigma\sigma}, \quad (1)$$

where $\sigma = \uparrow, \downarrow$ is the index of spin; G^r and G^a are retarded and advanced Green's functions of the system; Γ_{α} ($\alpha = L, R$) is linewidth function which describes the coupling between the α lead and the scattering region. Under finite bias voltage, the spin resolved current is calculated by the Landauer-Büttiker formula,

$$I_{\sigma} = -\frac{e}{h} \int_{-\infty}^{+\infty} dE [f_L(E - \mu_L) - f_R(E - \mu_R)] T_{\sigma}(E), \quad (2)$$

where f_{α} is the Fermi distribution function of lead α with chemical potential μ_{α} .

The spin polarization of the system is defined as

$$SP = \frac{I_{\uparrow} - I_{\downarrow}}{I_{\uparrow} + I_{\downarrow}} \times 100\%. \quad (3)$$

TMR is defined as,

$$TMR = \frac{I_{\sigma}^{FM} - I_{\sigma}^{AFM}}{I_{\sigma}^{AFM}}, \quad (4)$$

where $I_{\sigma}^{FM} = I_{\sigma\uparrow}^{FM} + I_{\sigma\downarrow}^{FM}$ and $I_{\sigma}^{AFM} = I_{\sigma\uparrow}^{AFM} + I_{\sigma\downarrow}^{AFM}$. I_{σ}^{FM} (I_{σ}^{AFM}) is the spin polarized current of FM (AFM) configuration, where the orientations of the magnetic moments in both leads are parallel (anti-parallel). When the bias voltage is small enough, I_{σ} in Eq.(3) and Eq.(4) can be replaced by T_{σ} at Fermi level.

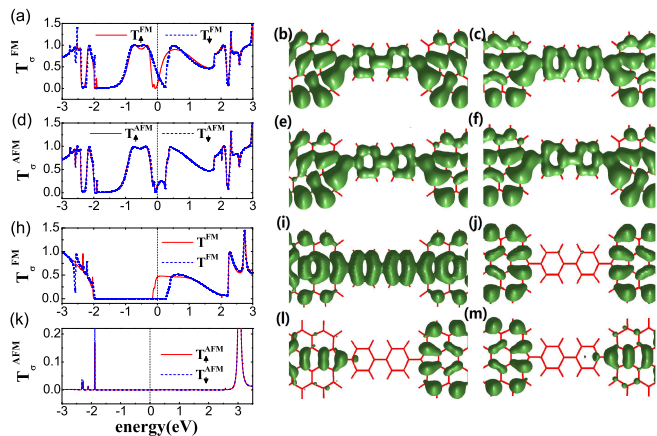


Fig. 2 (Color online) Spin resolved transmission coefficient T_σ at equilibrium ((a),(d),(h),(k)) and isosurface of scattering states at the Fermi level for spin up channel ((b),(e),(i),(l)) and spin down channel ((c),(f),(j),(m)) of biphenyl-ZGNR nanostructures ($M=2$, $N=4$). (a)-(c) are for FM configuration of dangling structure, (d)-(f) are for AFM configuration of dangling structure, (h)-(j) are for FM configuration of pentagon structure, and (k)-(m) are for AFM configuration of pentagon structure. In (a),(d),(h) and (k), the red solid curves and blue dash curves correspond to T_\uparrow and T_\downarrow , respectively. The Fermi level is set to zero indicated by the vertical dot lines.

3 Results and discussion

Firstly, we investigated TMR of the structures as shown in Fig.1 in the small bias limit (near equilibrium). Spin resolved transmission coefficients T_σ were calculated for both dangling structure and pentagon structure, which show completely different behaviors of TMR at equilibrium. For the dangling structure, T_σ is finite at Fermi level for both spins of FM (T_σ^{FM}) and AFM (T_σ^{AFM}) configurations (see Fig.2(a) and Fig.2(d)). For FM configuration of pentagon structure (see Fig.2(h)), T_\uparrow^{FM} is finite and T_\downarrow^{FM} is almost equal to zero when energy is between $-0.2eV$ and $0.5eV$, which gives large spin polarization around the Fermi level. Numerical results show that T_\uparrow^{FM} around the Fermi level is mainly contributed by the hybridization of the edge states of ZGNR and the re-normalized HOMO state of the biphenyl molecule. For AFM configuration of pentagon structure (see Fig.2(k)), a larger gap $\sim 5eV$ appears around the Fermi level for both T_\uparrow^{AFM} and T_\downarrow^{AFM} . From Eq.(4), TMR is found to be small for the dangling structure ($\sim 21\%$), while it is huge for the pentagon structure ($\sim 7.6 \times 10^4$ or $7.6 \times 10^6\%$) in small bias limit.

This TMR value is much larger than that proposed in other molecular MTJs¹⁵⁻¹⁸. It is necessary to confirm the generic property of huge TMR in such polyphenyl-ZGNR nanojunctions. We thus calculated the equilibrium transmission coefficients of other polyphenyl-ZGNR nanostructures by increas-

ing ZGNR width N and phenyl group number M . For the configuration with $N=4,6,8,10$, phenyl groups are placed close to or in the center line of graphene leads. While for another configuration with $N=10$ ($N=10'$), phenyl groups are placed close to one edge of graphene leads. Typical data are shown in Table 1 and general conclusion can be deduced. For all the dangling structures, TMR is always small at equilibrium (less than 100%). While for all the pentagon structures, TMR is always huge with magnitude roughly 10^4 .

To understand the physics essence behind huge TMR values of pentagon structures, scattering states at the Fermi level were calculated for both dangling structures and pentagon structures. We found that two reasons are responsible for the huge TMR. One is the mismatch of the scattering states from the leads and those in the central molecular region, and another one is the mismatch of the scattering states between two leads. The former induces a very small spin down transmission coefficient of FM configurations as shown in Fig.2(h) and the later contributes to very small transmission coefficients for both spin up and spin down electrons of AFM configurations as shown in Fig.2(k). As a result, a huge TMR is obtain according to Eq.(4). The detailed analysis is as follows. For the dangling structure with FM and AFM configurations, the extended p_y orbitals of the dangling carbon atoms take large overlap with the delocalized big π -orbital of biphenyl ring and graphene leads for both spin up and spin down electrons,⁴¹ which manifest that the spin up scattering state and the spin down scattering state at the Fermi level are well extended at biphenyl molecule and ZGNRs as shown in Fig.2(b), (c), (e) and (f). As a result, T_σ^{FM} and T_σ^{AFM} are finite and comparable, and thus TMR value is small. However, the situation is entirely different for the pentagon structures. For the spin up channel of FM configuration of the pentagon structure, extended π -orbitals are formed in both pentagon and biphenyl molecule. Due to the coplanar conformation of biphenyl molecule and ZGNRs, the overlap of π -orbitals takes a maximum value and π electrons can easily go through the system as shown in Fig.2(i), which gives rise to a large spin up transmission coefficient. Similar result has been obtained in previous investigation which indicated that the transmission coefficient is sensitively depends on the angle between the molecular planer and the graphene leads.⁴¹ While for the spin down channel of FM configuration, the scattering wave function is completely blocked in the biphenyl molecular region as shown in Fig.2(j) because of the mismatch of the orbital of biphenyl molecule to that of ZGNR leads. As a result, T_\downarrow^{FM} around the Fermi level is close to zero. The spin selection properties of transmission coefficient around the Fermi level has been reported in perfect ZGNRs.⁴² Furthermore, for the AFM configuration of the pentagon structure, the spin up (down) wave functions from left lead are orthogonal to that from right lead because of the spin splitting of spin up and

	$N (M=2)$					$M (N=4)$			
	4	6	8	10	$10'$	3	4	5	6
TMR I	0.21	0.28	0.35	0.38	0.92	0.42	0.63	0.38	0.54
TMR II	7.4×10^4	6.2×10^4	5.4×10^4	3.6×10^4	2.7×10^4	1.2×10^4	3.3×10^4	5.2×10^4	7.9×10^4

Table 1 TMR of dangling structures (TMR I) and pentagon structures (TMR II) with different ZGNR widths N and different phenyl group numbers M .

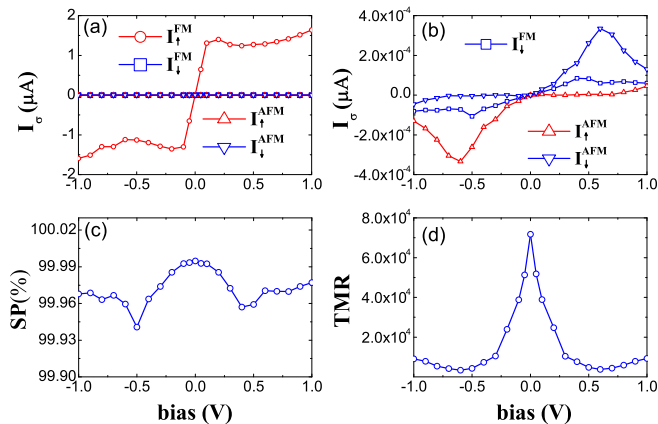


Fig. 3 (Color online) (a): Spin polarized current I_σ versus bias voltage for FM and AFM configurations of pentagon structure ($M=2$, $N=4$). I_σ^{FM} , I_σ^{FM} , I_σ^{AFM} and I_σ^{AFM} are plotted by curves with circle, square, up-triangle and down-triangle on them, respectively. (b): Zoom in of (a) for I_σ^{FM} , I_σ^{AFM} and I_σ^{AFM} . (c): The spin polarization SP versus bias voltage for the FM configuration. (d): TMR versus bias voltage.

spin down density of states around the Fermi level. Therefore, scattering states are barely distributed on the molecule for both spins (see Fig.2(l) and Fig.2(m)) and the transmission coefficients are close to zero at the Fermi level. As a result, a remarkably huge TMR is obtained. Our numerical results and theoretical analysis support that the pentagon-connecting formation between the molecule and ZGNRs is critical for the remarkably huge TMR.

In the following, we will focus on the pentagon configuration of biphenyl-ZGNRs MTJ to investigate the influence of bias voltage and gate voltage to the huge TMR. Fig.3(a) and Fig.3(b) show the spin polarized current versus bias voltage $\Delta V = V_L - V_R$ for FM and AFM configurations. We see that I_σ^{FM} is almost zero for all biases, while I_σ^{FM} increases linearly to $\sim 1.5 \mu A$ when the bias voltage increases from zero to about 0.15V and then I_σ^{FM} saturates around 1.2 to 1.6 μA upon further increase of bias voltage. As a result, spin polarization of FM configuration reaches $\sim 100\%$ (see Fig.3(c)) independent of bias voltage. This suggests that the pentagon structure of biphenyl-graphene nanojunction is a perfect spin filter. More-

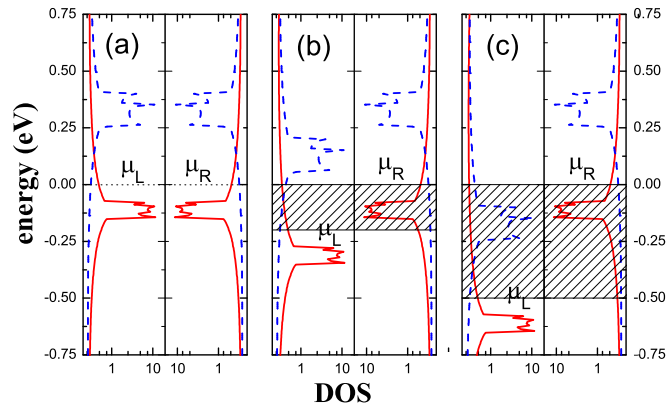


Fig. 4 (Color online) The spin polarized DOS of left lead and right lead versus bias voltage: (a) zero bias, (b) a smaller bias $\Delta V=0.2V$, and (c) a larger bias $\Delta V=0.5V$. In each case, the left panel indicates the DOS of left lead and the right panel indicates the DOS of right lead. Spin up DOS and spin down DOS are plotted by the red solid curve and blue dash curve, respectively. The shadow regions in (b) and (c) correspond to the mismatch between the chemical potentials of left lead μ_L and right lead μ_R , where $\mu_L = eV_L$ and $\mu_R = 0$.

over, although the bias dependent behavior of I_σ^{AFM} is similar to I_σ^{FM} as shown in Fig.3(d), its value is much smaller than I_σ^{FM} for all the bias voltages. From Eq.(4), huge TMR is obtained with the maximum value $\sim 7 \times 10^4$ at zero bias voltage. From Fig.3(d) we see that TMR decays with the increase of the bias voltage, but its minimum value is still $\sim 4 \times 10^3$ ($4 \times 10^5\%$) in the bias range $(-1V, 1V)$. This TMR is still much larger than that of the conventional spin valve device at the same bias^{6,10,11,18}. It shows that our biphenyl-graphene nanojunction is a robust and an ideal spin valve as well as MTJ device.

In the following, we analyze the physics of TMR behavior versus bias voltage as shown in Fig.3(d). The decay of TMR versus bias voltage is transparently from the decrease of growth rate of I_σ^{FM} (see Fig.3(a)) and quick increase of I_σ^{AFM} (in Fig.3(b)) under finite bias voltage. We firstly analyze the behavior of I_σ^{FM} versus bias voltage which can be understood by analyzing the spin resolved DOS of the left and the right ZGNR lead. Due to parallel arrangement of magnetic moments on both edges of ZGNR, spin up edge state and spin

down edge state are split. At equilibrium, both leads contribute to the same DOS as shown in Fig.4(a), where the spin up DOS peak is below the Fermi level and the spin down DOS peak is above the Fermi level. At the Fermi level ($E_f = 0$), spin up DOS is much larger than spin down DOS. This explains the spin filtering property of the device in the small bias limit to some extent. With increase of bias voltage, chemical potential of the left lead is shifted lower than that of the right lead as shown in Fig.4(b) and (c). When $\Delta V < 0.15V$, the peak of spin up DOS of the right lead gradually enters the energy window (μ_L, μ_R). Rapid increase of I_{\uparrow}^{FM} at low bias voltage is due to the energy integration in this energy window. When $\Delta V \sim 0.15V$, edge state of spin up channel in the right lead completely enters the energy window and hence I_{\uparrow}^{FM} reaches its maximum. With further increase of bias voltage from $\Delta V \sim 0.15V$, spin up DOS of both leads between μ_L and μ_R is barely changed, and therefore I_{\uparrow}^{FM} keeps $\sim 1.5\mu A$ with ΔV changed from $0.15V$ to $1V$. In the following, we discuss the behavior of I_{σ}^{AFM} versus bias voltage as shown in Fig.3(b). Although T_{\uparrow}^{AFM} and T_{\downarrow}^{AFM} are not resolved at zero bias as show in Fig.2(k), T_{\downarrow}^{AFM} shifts to the smaller energy with increase of bias, while T_{\uparrow}^{AFM} shifts to the larger energy with increase of bias. $T_{\downarrow}^{AFM}(E_f)$ increases with increase of bias, while $T_{\uparrow}^{AFM}(E_f)$ increases with decrease of bias, although they are still very small. When ΔV reaches $\sim 0.6V$, $\int_{E_f - e\Delta V}^{E_f} T_{\downarrow}^{AFM}(E)dE$ reaches the maximum value and furthermore the largest I_{\downarrow}^{AFM} . Further increase of bias voltage will decrease the value of transmission coefficient around the Fermi level, and therefore I_{\downarrow}^{AFM} decreases again. Similar discussion explains the increasing behavior of I_{\uparrow}^{AFM} versus negative bias voltage as shown in Fig.3(b). The bias controlled spin selection of electric current through AFM configuration of graphene based MTJ has been reported and the behavior is attributed to the orbital symmetry of spin subbands.^{42,43} Since the increasing rate of I_{σ}^{AFM} is much faster than that of I_{\uparrow}^{FM} , decreasing TMR versus bias voltage is observed as shown in Fig.3(d).

Supplying a gate voltage to electronic device is a conventional method to control the effective channel numbers for electric transport. In the following, we explore the gate controlled spin and electric behaviors in biphenyl-graphene molecular junction. To achieve that, an initial ramp electric field is supplied between the upper and the lower boundaries of scattering region to model gate voltage. The final gate controlled effective potential of the system is determined self-consistently from first principles.^{32,33} Fig.5(a) shows the spin polarized transmission coefficient T_{σ} at the Fermi level versus gate voltage V_g for both FM and AFM configurations with pentagon-connecting formation of biphenyl-graphene nanostructures. T_{\uparrow}^{FM} is much larger than T_{\downarrow}^{FM} , T_{\uparrow}^{AFM} , and T_{\downarrow}^{AFM}

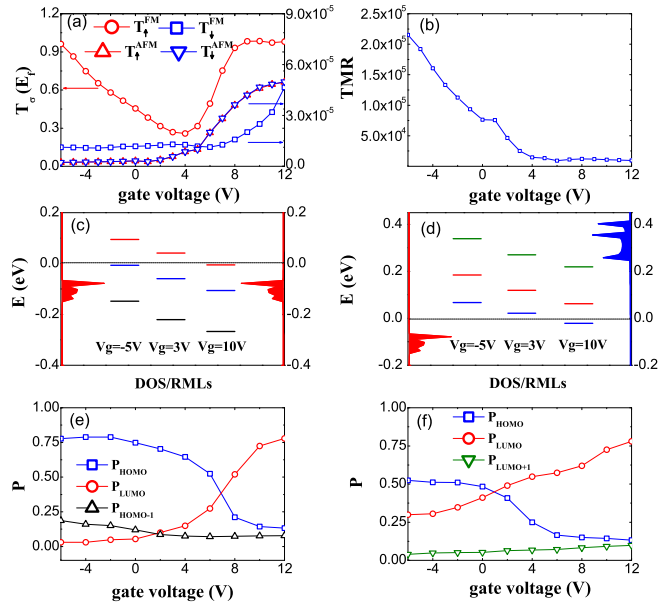


Fig. 5 (Color online) (a) Spin polarized transmission coefficient T_{σ} at the Fermi level for FM and AFM configurations of pentagon structure ($M=2, N=4$) versus gate voltage. (b) TMR versus gate voltage. (c) Spin up DOS of both leads (left and right red blank maps), and spin up RMLs of *isolated* biphenyl molecule (short lines) for FM configuration of pentagon structure under different gate voltage. The red short lines, blue short lines, and black short lines indicate the RMLs of LUMO, HOMO, and HOMO-1 levels, respectively. The left, center, and right three columns of lines correspond the RMLs under $V_g = -5V, V_g = 3V, V_g = 10V$, respectively. (d) Similar to panel (c) but for AFM configuration. The green short lines, red short lines, and blue short lines indicate the RMLs of LUMO+1, LUMO, and HOMO levels, respectively. (e) P_{LUMO} , P_{HOMO} , and P_{HOMO-1} versus gate voltage for spin up channel of FM configuration. (f) P_{LUMO} , P_{HOMO} , and P_{LUMO+1} versus gate voltage for spin up channel of AFM configuration.

by roughly four to five orders of magnitude under all the gate voltage. As a result, spin polarization is very close to 100% for FM configuration and is not very sensitive to gate voltage. T_{\uparrow}^{FM} decreases firstly and then increases versus gate voltage from $-6V$ to $12V$, while T_{\downarrow}^{FM} , T_{\uparrow}^{AFM} , and T_{\downarrow}^{AFM} show roughly nonlinear increasing behavior although their values are still very small. Due to spin asymmetry, T_{\uparrow}^{AFM} and T_{\downarrow}^{AFM} show the same behavior versus gate voltage at equilibrium. According to Eq.(4), TMR decreases from $\sim 2.2 \times 10^5$ to 1×10^4 with gate voltage increasing from $-6V$ to $5V$, and then TMR keeps roughly 1×10^4 with further increase of gate voltage as shown in Fig.5(b).

To understand the gate controlled behavior of spin resolved conductance, we calculated the renormalized molecular levels (RMLs) of *isolated* biphenyl molecule for each spin of FM and AFM configurations under different gate voltage, and

then analyze the relationship between the RMLs and conductance of system. Numerical results show that the conductance is mostly dominated by the RMLs close to the Fermi level, *i.e.*, LUMO+1, LUMO, HOMO and HOMO-1. We firstly analyze the gate controlled behavior of T_{\uparrow}^{FM} and the corresponding RMLs. Fig.5(c) shows the LUMO, HOMO, and HOMO-1 RMLs of spin up channel of FM configuration with gate voltage $V_g = -5V, 3V$ and $10V$. When $V_g = -5V$, HOMO level is very close to the Fermi level ($E_{HOMO} = -0.017eV$) and therefore T_{\uparrow}^{FM} is large. With increase of gate voltage from $-5V$ to $3V$, HOMO level is pushed gradually far away from the Fermi level, so T_{\uparrow}^{FM} decreases. With further increase of gate voltage to $V_g = 10V$, LUMO level is pushed down close to the Fermi level with $E_{LUMO} = -0.012eV$ and its contribution to the transmission coefficient become important. As a result, T_{\uparrow}^{FM} increases again. Then we analyze the gate controlled behavior between the RMLs and T_{σ}^{AFM} with $\sigma = \uparrow, \downarrow$. Although T_{σ}^{AFM} is always small under all the gate voltage due to the mismatch of the scattering states between two leads as aforementioned, we can still track some clues of the increasing of T_{σ}^{AFM} versus gate voltage as shown in Fig.5(a). When V_g is negative, all the RMLs are far away from the DOS peak of left lead as shown in Fig.5(d). With increase of gate voltage, all the RMLs are pushed down with HOMO level across the Fermi level. Therefore, T_{σ}^{AFM} is somewhat increases.

Using the scattering state projection technique,^{32,33} we can quantitatively estimate the contribution of each RMLs to the transmission coefficient by projecting the scattering state at the Fermi level to each RMLs as follows,

$$P_i = |\langle \phi_i | \Psi(E) \rangle|^2. \quad (5)$$

Here ϕ_i is the i -th renormalized eigenstate of the biphenyl molecule and $\Psi(E)$ is the scattering state at energy E of the system. P_i gives the information of which molecular state is more important for the transmission coefficient at energy E . As shown in Fig.5(e), when gate voltage is less than $7V$, T_{\uparrow}^{FM} is mostly contributed by HOMO state with decreasing P_{HOMO} value. While, with further increase of gate voltage from $7V$ to $12V$, LUMO state becomes more important and P_{LUMO} is largely increased. This method can also be used to quantitatively analyze the contribution to gate controlled transmission coefficient of AFM configuration as shown in Fig.5(f), where the small value of T_{σ}^{AFM} is mostly contributed by LUMO level with increasing values and HOMO level with decreasing values versus gate voltage. Finally, we need mention that although the gate voltage seems large in our calculation, the gating efficiency to the device is less than 1% as shown in Fig.5(c) and (d) because only a few percent of electric field lines pass through the device while most of the field lines goes to the leads, which is accordant with previous investigation^{34,35}.

4 Summary

In summary, we investigated the spin resolved quantum transport properties of polyphenyl-ZGNR MTJs by first principles calculation. For the structures with dangling-connecting formation, TMR is small. While for the structures with pentagon-connecting formation which is numerically proved more stable, TMR as large as $\sim 10^5$ is obtained and spin polarization can reach $\sim 100\%$. Scattering states at the Fermi level of each formation were calculated to explain this phenomenon of huge TMR, which indicate that the huge TMR is determined by two mismatches. One is the mismatch of the scattering states in the leads and in the scattering region, and another one is the mismatch of the scattering states between two leads around the Fermi level. Numerical results show that the remarkably huge TMR survives in a robust way, which is generic for all the pentagon-connecting formation of polyphenyl-ZGNR MTJs with different length of polyphenyl molecule and different width of ZGNRs. Moreover, this huge TMR is not significantly affected by external bias and gate voltage. A reasonable explanation is given to this phenomenon by using the scattering state projection technique.

Acknowledgments. This work was supported by National Natural Science Foundation of China (11304205, 11374246) and Natural Science Foundation of Shenzhen (JCYJ20130326111836781).

References

- 1 W.H. Butler, X.G. Zhang, T.C. Schulthess and J.M. MacLaren, *Phys. Rev. B: Condens. Matter*, 2001, **63**, 054416.
- 2 J. Mathon and A. Umerski, *Phys. Rev. B: Condens. Matter*, 2001, **63**, 220403.
- 3 J.S. Moodera, L.R. Kinder, T.M. Wong and R. Meservey, *Phys. Rev. Lett.*, 1995, **74**, 3273.
- 4 T. Miyazaki and N. Tezuka, *J. Magn. Magn. Mater.*, 1995, **139**, L231.
- 5 B.G. Park, T. Banerjee, J.C. Lodder and R. Jansen, *Phys. Rev. Lett.*, 2007, **99**, 217206.
- 6 S. Yuasa, T. Nagahama, A. Fukushima, Y. Suzuki and K. Ando, *Nat. Mater.*, 2004, **3**, 868.
- 7 S.S.P. Parkin, C. Kaiser, A. Panchula, P.M. Rice, B. Hughes, M. Samant and S.H. Yang, *Nat. Mater.*, 2004, **3**, 862.
- 8 L.M. Loong, X.P. Qiu, Z.P. Neo, P. Deorani, Y. Wu, C.S. Bhatia, M. Saeys and H. Yang, *Sci. Rep.*, 2014, **4**, 6505.
- 9 S. Ikeda, J. Hayakawa, Y. Ashizawa, Y.M. Lee, K. Miura, H. Hasegawa, M. Tsunoda, F. Matsukura and H. Ohno, *Appl. Phys. Lett.*, 2008, **93**, 082508.
- 10 Q.Y. Ke, K. Xia and H. Guo, *Phys. Rev. Lett.*, 2010, **105**, 236801.
- 11 L.L. Tao, S.H. Liang, D.P. Liu, H.X. Wei, J. Wang and X.F. Han, *Appl. Phys. Lett.*, 2014, **104**, 172406.
- 12 R.N. Mahato, H. Lulf, M.H. Siekman, S.P. Kersten, P.A. Bobbert, M.P. de Jong, L. De Cola and W.G. van der Wiel, *Science*, 2013, **341**, 6143.
- 13 H.B. Gu, X. Zhang, H.G. Wei, Y.D. Huang, S.Y. Wei and Z.H. Guo, *Chem. Soc. Rev.*, 2013, **42**, 5907.
- 14 B. Wang, Y. Zhu, W. Ren, J. Wang, and H. Guo, *Phys. Rev. B* 2007, **75**, 235415.

- 15 A.R. Rocha, V.M. Garcia-Suarez, S.W. Bailey, C.J. Labert, J. Ferrer and S. Sanvito, *Nat. Mater.*, 2005, **4**, 335.
- 16 F.X. Zu, Z.L. Liu, K.L. Yao, G.Y. Gao, H.H. Fu, S.C. Zhu, Y. Ni and L. Peng, *Sci. Rep.*, 2014, **4**, 4838.
- 17 Y. Ni, K.L. Yao, C.Q. Tang, G.Y. Gao, H.H. Fu and S.C. Zhu, *Rsc. Adv.*, 2014, **4**, 18522.
- 18 C. Cao, Y. Wang, H.P. Cheng and J.Z. Jiang, *Appl. Phys. Lett.*, 2011, **99**, 073110.
- 19 S. Mandal and R. Pati, *Acs Nano*, 2012, **6**, 3580.
- 20 K.S. Novoselov, A.K. Geim, S.V. Morozov, D. Jiang, M.I. Katsnelson, I.V. Grigorieva, S.V. Dubonos and A.A. Firsov, *Nature*, 2005, **438**, 197.
- 21 A.K. Geim and K.S. Novoselov, *Nat. Mater.*, 2007, **6**, 183.
- 22 F. Schwierz, *Nat. Nanotechnol.*, 2010, **5**, 487.
- 23 K. Nakada, M. Fujita, G. Dresselhaus and M.S. Dresselhaus, *Phys. Rev. B*, 1996, **54**, 17954.
- 24 W.Y. Kim and K.S. Kim, *Nat. Nanotechnol.*, 2008, **3**, 408.
- 25 J. Kang, F.M. Wu, S.S. Li, J.B. Xia and J.B. Li, *Appl. Phys. Lett.*, 2012, **100**, 153102.
- 26 G. Kresse and J. Furthmuller, *Phys. Rev. B*, 1996, **54**, 11169.
- 27 There are totally 146 atoms in the scattering region for both pentagon connected structure and dangling connected structure. The total energy is -33037.8345eV for the former and -33029.7759eV for the later. The total energy difference between these two structures is about 55meV per atom.
- 28 H. Lee, Y. Son, N. Park, S. Han and J. Yu, *Phys. Rev. B*, 2005, **72**, 174431.
- 29 Y.W. Son, M.L. Cohen and S.G. Louie, *Nature*, 2006, **444**, 347.
- 30 X. Wang, Y. Ouyang, X. Li, H. Wang, J. Guo and H. Dai, *Phys. Rev. Lett.*, 2008, **100**, 206803.
- 31 X.F. Guo, J.P. Small, J.E. Klare, Y.L. Wang, M.S. Purewal, I.W. Tam, B.H. Hong, R. Caldwell, L.M. Huang, S. O'Brien, J.M. Yan, R. Breslow, S.J. Wind, J. Hone, P. Kim and C. Nuckolls, *Science*, 2006, **311**, 356.
- 32 D. Waldron, P. Haney, B. Larade, A. MacDonald and H. Guo, *Phys. Rev. Lett.*, 2006, **96**, 166804.
- 33 D. Waldron, V. Timoshevskii, Y. Hu, K. Xia and H. Guo, *Phys. Rev. Lett.*, 2006, **97**, 226802.
- 34 J. Taylor, H. Guo and J. Wang, *Phys. Rev. B*, 2001, **63**, 245407.
- 35 J. Taylor, H. Guo and J. Wang, *Phys. Rev. B*, 2001, **63**, 121104.
- 36 P. Ordejón, E. Artacho and J.M. Soler, *Phys. Rev. B*, 1996, **53**, 10441.
- 37 J.M. Soler, E. Artacho, J.D. Gale, A. Garcia, J. Junquera, P. Ordejon and D. Sanchez-Portal, *J. Phys: Condens Matter.*, 2002, **14**, 2745.
- 38 U. Vonbarth and L. Hedin, *J. Phys. C*, 1972, **5**, 1629.
- 39 O. Gunnarsson and B.I. Lundqvist, *Phys. Rev. B*, 1996, **13**, 4274.
- 40 A.K. Rajagopal, *J. Phys. C*, 1978, **11**, L943.
- 41 H.Q. Wan, B. Zhou, X.W. Chen, C.Q. Sun and G.H. Zhou, *J. Phys. Chem. C*, 2012, **116**, 2570; H.Q. Wan, Y. Xu and G.H. Zhou, *J. Chem. Phys.*, 2012, **136**, 184704.
- 42 B. Wang, J. Wang and H. Guo, *Phys. Rev. B*, 2009, **79**, 165417.
- 43 M.G. Zeng, L. Shen, Y.Q. Cai, Z.D. Sha and Y.P. Feng, *Appl. Phys. Lett.*, 2010, **96**, 042104.